Efficient Geometric Correction Workflow for Airborne Hyperspectral Images through DEM-Driven Correction Techniques

Junchuan Yu[1,2], Yichuan Li[1], Daqing Ge[1,2], Yangyang Chen[1,2], Qiong Wu[1,2], Yanni Ma[1,2]

[1] China Aero Geophysical Survey and Remote Sensing Center for Natural Resources, China – {yujunchuan, lyichuan, gedaqing, chenyangyang, wuqiong, mayanni} @mail.cgs.gov.cn

[2] Technology Innovation Center for Geohazard Identification and Monitoring with Earth Observation System, Ministry of Natural Resources, China

Keywords: Aerial, Hyperspectral, Geometric correction, DEM, Local matching.

Abstract

Geometric correction, a pivotal step in the preprocessing of airborne remote sensing imagery, is critical for ensuring the accuracy of subsequent quantitative analyses. Achieving precise and efficient geometric correction for airborne hyperspectral data remains a significant challenge in the field. This study presents a new method for system-level and fine-scale geometric correction of uncontrolled airborne images utilizing DEM data, which integrates forward and inverse transformation algorithms. Furthermore, an optimized workflow is proposed to facilitate the processing of large-scale hyperspectral datasets. The effectiveness of the proposed method is demonstrated through an application analysis using airborne HyMap imagery, with experimental outcomes indicating high application accuracy and enhanced processing efficiency.

1. Introduction

Aerial remote sensing, characterized by its strong autonomy, high precision, efficiency, and flexibility, has emerged as an effective means for rapidly acquiring high-accuracy remote sensing data. As the demand for remote sensing data evolves towards high spatial, temporal, and spectral resolutions—often referred to as the "three highs"—the application of airborne hyperspectral imaging has garnered increasing attention. The rise of airborne hyperspectral imaging has led to notable advancements in environmental monitoring, agriculture, and geological mapping. Geometric correction, a critical component of remote sensing data processing, is pivotal in determining the precision of subsequent quantitative applications. Compared to satellite remote sensing, the imaging environment and the extent and patterns of geometric distortion in aerial remote sensing differ significantly. Typically, aerial remote sensing operates at altitudes ranging from 1000 to 3000 meters, where the intense and rapidly changing atmospheric turbulence leads to frequent sensor attitude variations. This results in geometric errors in aerial remote sensing that are considerably greater than those in satellite remote sensing (Zhang et al., 2001). Consequently, geometric correction models suitable for satellite imagery cannot be simply adapted for application to aerial remote sensing imagery without modification.

In general, geometric correction models for aerial remote sensing can be categorized into two types: forward transformation and inverse transformation (Li et al., 1991). Inverse transformation employs ground control points to digitally simulate the geometric distortion process of the imagery, establishing a correspondence between the distorted image space and the corrected space to achieve geometric correction. This method is suitable for correcting non-systematic geometric distortions in the imagery, such as the traditional rubber-sheet method (Bähr 1976, Goshtasby 1988), piecewise polynomial method (McGwire 1996), and correlation matching algorithm (Devereux et al., 1990, Reulke et al., 1997). These methods rely on a significant number of control points, and their application accuracy often depends on the geometric precision of the reference imagery (Gregory et al., 1999). Forward transformation, on the other hand, calculates the true coordinates of each pixel based on known sensor position and attitude data, such as the Parametric Geocoding method (Meyer 1994, Schläpfer et al. 1998a/b, 2002). This approach has been successfully applied to various airborne sensors, including AISA, AVIRIS, and CASI. However, due to the complexity of the data acquisition process in airborne systems, the involved parameters cannot be accurately estimated, and thus are typically used for correcting systematic geometric distortions in the imagery. Previous research has primarily focused on the applicability and model accuracy of geometric correction methods for remote sensing data. However, when implementing these methods in practical scenarios, it's important to also consider the processing efficiency, which is especially critical when handling large volumes of hyperspectral data. Experiments demonstrate that airborne hyperspectral dataset covering 2000 km^2 at a spatial resolution of 1 meter can generate several terabytes of data. The ability to quickly and effectively process these massive amounts of data is crucial for maximizing the utility of methods and meeting the needs of various applications in different fields.

Addressing these issues, this paper builds upon previous work and proposes a geometric correction method that combines forward and inverse transformations based on DEM data. The method is evaluated using HyMap data for geometric correction experiments and accuracy assessment. Furthermore, optimization strategies are presented to address the low data processing efficiency caused by the large volume of hyperspectral data.

2. Methods

2.1 Basic Geometric Correction Based on DEM Data

The core of the geometric correction method for airborne imaging spectrometers using DEM data is to calculate the sensor's scanning vector based on the acquired geometric parameters. Due to the influence of atmospheric turbulence, the airborne photoelectric platform may experience pitch, roll, and yaw, leading to changes in the relative position of the starting point relative to the aircraft coordinate system (Figure 2), i.e., the roll angle (φ), pitch angle (θ), and yaw angle (ψ) (Li et al., 2016). Initially, it is assumed that at a certain altitude H, the sensor's flight attitude angles are all zero, which is considered the initial state. At this time, the scanning vector is denoted as L_i' For a swing-type sensor, the change in the X-axis (Xi) depends on the scanning direction and angle $s{\cdot}tan\theta$, while the Y-axis (Yi) remains unchanged, Yi is 0, and the Z-axis (Zi) is -1.

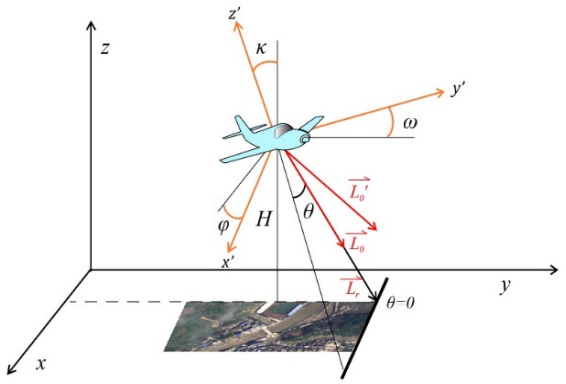

Figure 1. The diagram of sensor attitude parameters and scan vector geometry

When the sensor is acquiring data, the flight attitude angles are variable, and the scanning vector is denoted as L_0'. By obtaining the three attitude parameters, the transformation relationship between the aircraft coordinate system and the initial coordinate system can be constructed, as shown in Equation (1):

$$L_0 = R \cdot P \cdot H \cdot L_1 \tag{1}$$

Where R, P, and H represent the transformation matrices for the roll angle, pitch angle, and yaw angle, respectively, expanded as shown in Equations (2) and (3):

$$\begin{bmatrix} L_{0x} \\ L_{0y} \\ L_{0z} \end{bmatrix} = \begin{bmatrix} \cos\omega & 0 & -\sin\omega \\ 0 & 1 & 0 \\ \sin\omega & 0 & \sin\omega \end{bmatrix} \begin{bmatrix} \cos\omega & 0 & -\sin\omega \\ 0 & 1 & 0 \\ \sin\omega & 0 & \sin\omega \end{bmatrix} \begin{bmatrix} \cos\omega & 0 & -\sin\omega \\ 0 & 1 & 0 \\ \sin\omega & 0 & \sin\omega \end{bmatrix} \cdot \begin{bmatrix} X_i \\ Y_i \\ Z_i \end{bmatrix} \tag{2}$$

$$\begin{bmatrix} L_{0x} \\ L_{0y} \\ L_{0z} \end{bmatrix} = \begin{bmatrix} \cos\omega\cos\kappa - \sin\omega\sin\varphi\sin\kappa & 0 & -\sin\omega\cos\varphi \\ -\cos\varphi\sin\kappa & \cos\varphi\cos\kappa & \sin\varphi \\ \sin\omega\cos\kappa + \cos\omega\sin\varphi\sin\kappa & \sin\varphi & \cos\omega\cos\varphi \end{bmatrix} \cdot \begin{bmatrix} s\cdot\tan\theta \\ 0 \\ -1 \end{bmatrix} \tag{3}$$

$$L_r = \frac{-h}{Z_{\text{initial}}} \cdot L_0 = \frac{-h}{(\sin\omega\cos\kappa + \cos\omega\sin\varphi\sin\kappa)\cdot s\cdot\tan\theta - \cos\omega\cdot\cos\varphi} \cdot L_r \tag{4}$$

The scanning vector calculated at altitude H still needs to be converted to its actual value (Konecny G and Lehmann G, 1984), thus obtaining the true scanning vector for each pixel in the sensor's scan line. The conversion method is shown in Equation (4).

$$\max\left(\cos < \overrightarrow{L_d}, \overrightarrow{L_r} >\right) \to 1 \tag{5}$$

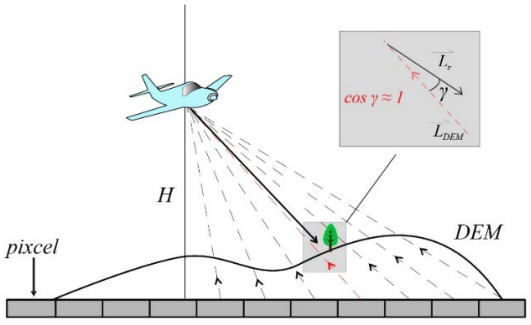

Figure 2. The diagram of DEM-based geometric correction method

As illustrated in Figure 2, given the DEM data and sensor GPS data, the scanning vector L_d' for any DEM pixel relative to the sensor can be calculated. By employing Equation (5), the true coordinate information corresponding to the sensor's scan pixel for the DEM pixel can be obtained by identifying the scanning vector L_d' that is closest to the reference scanning vector L_r'.

2.2 Fine Geometric Correction

Based on Polynomial Fitting Although the above method can quickly perform geometric correction, its accuracy is limited by the geometric precision of the DEM data and the accuracy of the sensor acquisition parameters. Further correction is needed to eliminate the impact of non-systematic geometric distortions. Polynomial correction is a commonly used geometric correction method, which assumes that the geometric errors of the image are the result of a combination of basic deformations such as rotation, translation, affine, scaling, and skew. Therefore, the coordinate relationship between corresponding points before and after the correction can be expressed using a bivariate n-order polynomial:

$$\begin{cases} \mathrm{x} = \sum_{i=0}^{n}\sum_{j=0}^{n-i} a_{ij}\mu_i\nu_i \\ y = \sum_{i=0}^{n}\sum_{j=0}^{n-i} b_{ij}\mu_i\nu_i \end{cases} \tag{6}$$

Where x and y represent the coordinates of the image before the transformation, while u and v represent the coordinates after the transformation. The coefficients aij and bij are the parameters of the equation, and n denotes the order of the polynomial. This approach circumvents the spatial geometric process of imaging by directly simulating the image distortion through mathematical modelling. The selection of control points is primarily based on an automatic method that relies on pixel-level values, with manual assistance required in some cases. The control points should be distributed as evenly as possible, as a denser distribution of control points leads to higher accuracy.

3. Geometric Correction Experiments

3.1 HyMap Airborne Hyperspectral Data

The HyMap sensor, developed by Integrated Spectronics Pty Ltd. in Australia and operated by HyVista, is a mainstream commercial airborne hyperspectral imaging system. The new generation HyMapC sensor is equipped with four detectors, with detailed parameters listed in Table 1. The working wavelength range has been increased from 124 to 144 bands, covering the visible to near-infrared spectrum with a spectral resolution of 15-20nm. The total field of view is 60°, with 668 scan lines per image, and the signal-to-noise ratio reaches 600~1000.

Sensor	Wavelength (nm)	Bandwidth (nm)	Sampling Interval (nm)	Band Number
VIS	400~905	15~16	15	36
NIR	880~1410	18~20	18	36
SWIR1	1400~1960	18~20	18	36
SWIR2	1950~2500	18~20	18	36

Table 1. Hymap Detector Parameter List

The data used in this study was acquired by the China Aero Geophysical Survey and Remote Sensing Center for Natural Resources on June 28, 2016, in the Lop Nur region of Xinjiang using the HyMap (C) airborne sensor. The spatial resolution of the data is 2.5 meters × 2.5 meters, with a flight altitude of 1.5 km. The raw data obtained by HyMap includes the original DN values, GPS data (latitude and longitude, altitude) for each scan line, and attitude parameters (heading angle, yaw angle, roll angle, pitch angle). Typically, spectral measurements of typical objects on the ground are also carried out synchronously. Before performing geometric correction on the raw data, it is necessary to first decompress the data and conduct quality checks, radiometric calibration, atmospheric correction, and other processing steps.

3.2 Results of Geometric Correction Experiments

Initially, the latitude and longitude values of each pixel were calculated using the sensor's GPS data, attitude parameters, and DEM data, and converted into a geographic lookup table file. Then, a system-level geometric correction was applied to the true-color three-band HyMap data, with the results shown in Figure 3a. The corrected image's geometric position is essentially accurate when compared to the background of the geometrically precise Resource Three data. However, non-systematic geometric errors can still be observed from the texture and direction of the water systems. By marking multiple corresponding ground objects, the geometric error was estimated to be about 5-10 pixels.

Due to the lack of high-accuracy DEM data, we can only use a 30-meter DEM for sampling to obtain a 2.5-meter DEM to meet the geometry correction requirements of the HYMAP data. Due to the high precision of DEM, which will improve the accuracy of local matching, insufficient resolution of DEM data is one of the major sources of error in this experiment. For the HyMap device, only one set of latitude and longitude information can be obtained within the same scan line, i.e., the coordinates at the nadir point. Interpolating the GPS data to estimate the coordinates of each pixel can also affect the result's precision. The method effectively eliminates systematic geometric errors without relying on control points and does not require further orthorectification due to the consideration of topographic factors. However, the experimental results also reflect that due to the complexity of the airborne data acquisition environment and the numerous influencing factors, relying solely on the forward transformation method is clearly insufficient to completely suppress non-systematic errors.

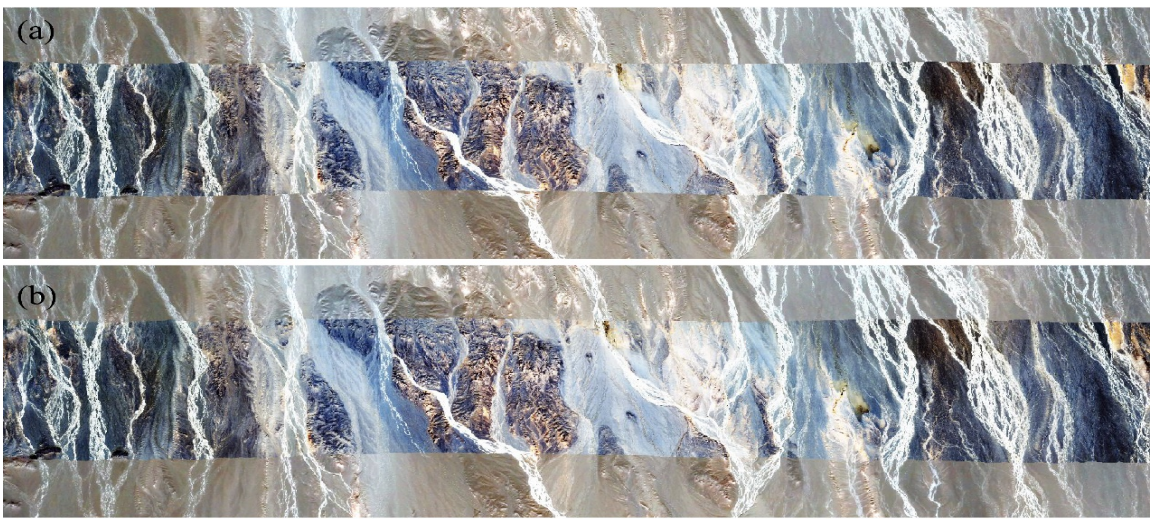

Figure 3. The diagram of Hymap system-level geometric correction result (a) and geometric fine correction result (b)

Following the system-level geometric correction, the preliminary geometrically corrected three-band true-color image was further refined using a bivariate quadratic polynomial for geometric fine correction, with the reference image being the geometrically precise reference data. A total of 180 control points were meticulously selected and evenly distributed throughout the image, as shown in Figure 4, to ensure a comprehensive coverage for the geometric fine correction process. The results, depicted in Figure 3b, demonstrate a high degree of geometric alignment with the reference image, indicating a successful correction. The geometric distortions, which were previously pronounced along the image edges and within linear textures, have been notably ameliorated, resulting in a markedly improved representation of the landscape's true geometry. The accuracy of the geometric fine correction was assessed using the Root Mean Square Error (RMSE), which is calculated using the following formula:

$$RMSE = \sqrt{\frac{1}{n}\sum_{i=1}^{n}\left[\left(x_i - x_i^{'}\right)^2 + \left(y_i - y_i^{'}\right)^2\right]} \quad (7)$$

Where n represents the number of control points, i denotes the index of the control point, with x_i and y_i representing the coordinates of the control point before correction, and $x_i^{'}$ and $y_i^{'}$ representing the coordinates of the control point after correction.

After the statistical analysis, the RMSE for all control points was calculated to be 0.96 pixels, effectively eliminating non-systematic geometric errors. The experimental results demonstrate that the combined forward and inverse transformation geometric correction method is well-suited for the geometric correction of airborne hyperspectral data.

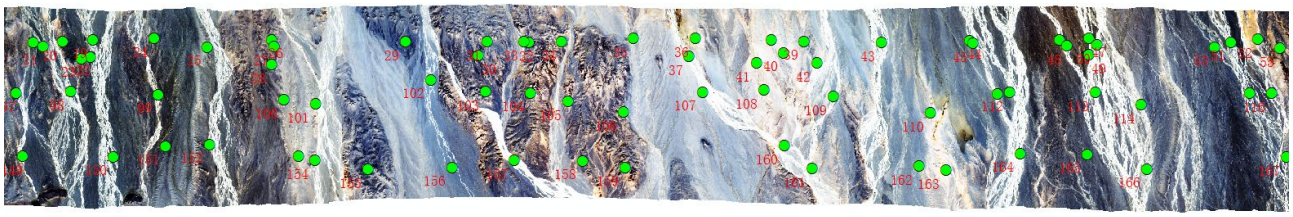

Figure 4. The diagram of geometric fine correction control point distribution

4. Rapid Geometric Correction Method for Hyperspectral Data

The method outlined previously has proven effective for three-band true-color images, delivering satisfactory outcomes. However, the challenge of processing efficiency becomes more pronounced when dealing with hyperspectral data, which encompasses hundreds of bands. To address this, it is crucial to not only choose the right data types and storage approaches that can effectively reduce the overall data volume but also to implement specific optimization techniques.

4.1 Local Matching Algorithm Based on Sliding Frame

In the aforementioned geometric correction method, a crucial step is to identify the DEM scanning vector $(L\_0)^{\rightarrow}$ that is closest to the sensor's scanning vector $(L\_d)^{\rightarrow}$, which corresponds to the coordinate where the cosine of the angle between the two scanning vectors is maximized. This optimal solution is found by calculating the coordinates at the point of maximum cosine. As shown in Figure 5, the vector $(L\_0)^{\rightarrow}$ is represented by an [m×n] matrix A, where m and n correspond to the length and width of the DEM, respectively. The vector $(L\_d)^{\rightarrow}$ is represented by an [ns×nl] matrix B, with ns and nl representing the number of columns and rows of the image, respectively. In practical calculations, determining the coordinates for each pixel requires iterating through the A matrix, resulting in a computationally intensive process of m×n×ns×nl operations to complete the calculation for the entire image.

In order to enhance the efficiency of the geometric correction process, especially when dealing with the extensive data sets inherent in hyperspectral imaging, a novel sliding frame-based local matching algorithm has been developed. This algorithm initiates the process by establishing initial pixel coordinates from an optimal solution. Subsequently, a radius R is defined, and a square sliding frame with a side length L, calculated as L=2R+1, is created with the initial pixel at its center.

The algorithm proceeds by moving through the Digital Elevation Model (DEM) incrementally, with each step being 1 pixel in size. This method effectively confines the computational scope to a localized area of L×L for each iteration, thereby narrowing down the search space and focusing on local optimization. By doing so, the algorithm achieves a substantial reduction in the computational burden, which is redefined as m×n×L×L operations, where m and n represent the dimensions of the image, and L is pragmatically set within the range of 10-20 to align with the specific demands of various engineering applications.

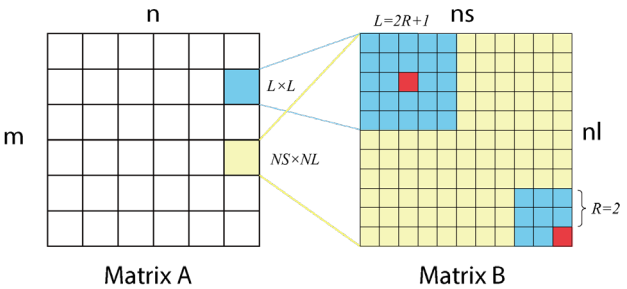

Figure 5. Schematic diagram of the sliding box-based local matching method

This localized approach not only expedites the processing time but also ensures that the algorithm remains responsive and adaptable to the dynamic nature of hyperspectral data. By tailoring the search parameters and focusing on relevant data subsets, the sliding frame-based local matching algorithm presents a robust and efficient solution for geometric correction in hyperspectral imaging applications.

4.2 Optimized Workflow

Figure 6a illustrates the traditional approach to geometric correction for a hyperspectral image with 144 bands, which necessitates two separate correction procedures to reach the final outcome. This will process all the 144 bands data in both system-level geometric correction and fine-level geometric correction processes. In fact, both geometric corrections are achieved by using control points. If we can obtain control points directly from non-geometric data to geometric precision-corrected data, it will greatly improve processing efficiency.

To solve this problem, we propose a new optimized geometry correction workflow which is shown in Figure 6b. First, we extract a single band with a high signal-to-noise ratio, perform system-level geometric correction using a GLT file, and then perform geometric fine correction on the system-level geometrically corrected data using reference data to obtain a control point file. Second, we use the control point file to geometrically correct the original GLT file to obtain a new control point file, which can be directly used to geometrically fine correct geometrically non-geometric hyperspectral data. The advantage of the latter is that the final geometric control points are obtained through system-level and fine geometric

corrections using a single-band image, and then a one-time geometric correction operation is performed on all bands, the optimized workflow efficiency compared to the original processing increased by 200%.

This method, under the premise of providing high-precision auxiliary data, can achieve automated and streamlined processing. In addition, maintaining data bit integrity during the calculation process will further improve computational efficiency. At the same time, combining distributed cluster systems and GPUs to build parallel processing workflows can provide a solution for fast geometric correction processing of large-scale hyperspectral data.

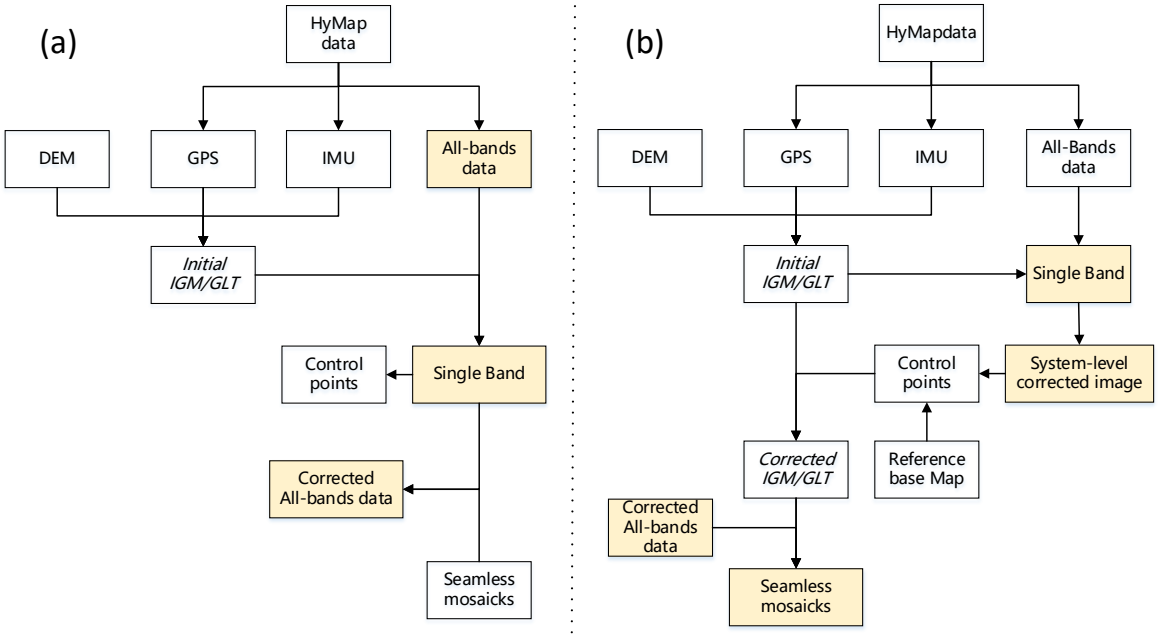

Figure 6. Diagram of the hyperspectral image geometric correction workflow before and after optimization

5. Conclusion

In conclusion, this research has effectively addressed the significant challenge of achieving precise and efficient geometric correction for airborne hyperspectral data, a critical step in preprocessing remote sensing imagery. By leveraging DEM data and integrating forward and inverse transformation algorithms, the study has presented a novel method for system-level and fine-scale geometric correction of airborne hyperspectral images. This method has been demonstrated through application analysis using HyMap data, which has resulted in high application accuracy and enhanced processing efficiency. The innovative aspect of this work lies in the optimized workflow, which simplifies the conventional process that typically requires two separate geometric corrections into a single operation. This streamlined approach not only reduces computational load but also enables automated and streamlined processing, which is particularly beneficial for handling large-scale hyperspectral datasets.

Despite the method's advantages, it is not without limitations. The accuracy of the geometric correction is contingent on the quality of the DEM data and the precision of the sensor acquisition parameters. Additionally, the lack of high-accuracy DEM data and the reliance on a 30-meter DEM for sampling to obtain a 2.5-meter DEM for geometry correction requirements introduce a potential source of error. Furthermore, the method's performance in diverse imaging environments and its scalability with varying data volumes remain areas for further investigation.

Future research will focus on refining the method to accommodate varying resolutions and larger datasets, as well as exploring the integration of machine learning techniques to automate the selection and placement of control points. This will further enhance the efficiency and accuracy of the geometric correction process. Additionally, the development of more sophisticated algorithms to handle the complex atmospheric turbulence effects on sensor attitude variations will be crucial for improving the method's applicability across different aerial remote sensing scenarios. By addressing these aspects, the research aims to contribute to the broader field of remote sensing by providing more reliable and efficient tools for data processing and analysis.

Acknowledgements

This work is supported by the National Key Research and Development Program of China (2021YFC3000400).

References

BAHR, H.P., 1976, Geometrische Modelle fur Abtasteraufzeichnungen von Erderkundungssatelliten. Bildmessung und Luftbildwesen, 44(5), 198-204.

Congalton, R.G., 1988, A comparison of sampling schemes used in generating error matrices for assessing the accuracy of maps generated from remotely sensed data. *Photogrammetric Engineering and Rermote Sensing*, 54(5), 593-600.

Schlapfer, D., and Richter, R., 2002. Geo-atmospheric processing of airborne imaging spectrometry data. part 1: parametric orthorectification. *International Journal of Remote Sensing*, 23(13), 2609-2630.

Devereux, B.J., Fuller R.M., Carter, L., and Parsell, R.J., 1990, Geometric correction of airborne scanner imagery by matching

delaunay triangles. *International Journal of Remote Sensing*, 11(12), 2237-2251.

Gregpru, S., Hhdges, P., and Elgy, J., 1999, The geometric correction of airborne line-scanner imagery. *4th International Airborne Remote Sensing Conference and Exhibition, ERIM, Ottawa,* CA, Vol. I, 178-185.

Konecny, G., and Lehmann, G., 1984, Photogrammetrie. *de Gruyter Lehrbuch, Walter de Gruyter,Berlin / New York*, 393.

Kruse, F.A., Boardman, J.W., Lefkoff, A. B., Young, J.M, et al. 1985. HyMap: an Australian hyperspectral sensor solving global problems-results from USA HyMap data acquisitions.

Li, S.K., 1991. Study on Remote Sensing Image Ground Orientation. Beijing : Mapping Publishing House Press.

Li, T.C., Liu, J.H, Zhou, Q.F., 2016. Geometric correction of Airborne Photoelectric Platform Images Based On Internal and External Parameters Of Camera. *Piezoelectric & Acoustooptics,* 38(1), 32-37.

McGwire, K.C., 1996. Cross-validated Assessment of Geometric Accuracy. *Photogrammetric Engineeringand Rermote Sensing*, 62(10), 1179-1187.

MEYER, P., 1994, A parametric approach for the Geocoding of Airborne Visible/Infrared Imaging Spectrometer (AVIRIS) Data in Rugged Terrain, *Remote Sensing of Environment*, 49, 118-130.

SCHLAPFER, D., MEYER, P., and ITTEN, K.I., 1998a, Parametric geocoding of AVIRIS data using a ground control point derived flightpath. *Summaries of the Seventh JPL Airborne Earth Science Workshop, JPL, Pasadena (CA)*, 1, 367-372.

SCHLAPFER, D., SCHAEPMAN, M., and ITTEN, K.I., 1998b, PARGE: Parametric geocoding based on GCP-calibrated auxiliary data. *Imaging Spectrometry IV*, SPIE 3438, 334-344.

Zhang, J.B., 2001. Study on Geometric correction of mid-low altitude Airborne Imaging spectral Imagery. *Uranium Geology*, 17(5), 307-313.

Zhu, L.P., 1994. Remote Sensing Geology. Beijing: Geological Publishing House.